A reaction surface Hamiltonian treatment of the double proton transfer of formic acid dimer

Norihiro Shida,[a] Paul F. Barbara,[b] and Jan Almlöf [b]
Department of Chemistry, University of Minnesota, Minneapolis, Minnesota 55455

(Received 25 June 1990; accepted 24 September 1990)

The double proton transfer reaction of the isolated formic acid dimer has been investigated within the reaction surface Hamiltonian framework, using a newly calculated three-dimensional *ab initio* potential energy surface. The symmetric (synchronous) proton movement, the asymmetric (asynchronous) proton movement and the relative motion of two formic acid molecules have been explicitly included in the calculation. The calculation gives a tunneling splitting of 0.004 cm^{-1}, which is considerably smaller than a previous theoretical prediction (0.3 cm^{-1}). An effective tunneling path has been calculated from the lowest vibrational eigenfunction of the reaction surface Hamiltonian, and the path deviates significantly from the minimum energy path on the potential energy surface. The new results are consistent with the conventional understanding of heavy–light–heavy mass combination reactions. The effective reaction path from this calculation reveals evidence of asymmetric proton movement. However, a synchronous double proton transfer is the major mode of reaction. Tunneling splittings for a few excited vibrational levels have also been calculated within the reaction surface Hamiltonian framework. Vibrational excitation of a large amplitude, heavy atom mode dramatically increases the tunneling splitting.

I. INTRODUCTION

The formic acid dimer (FAD) is the smallest carboxylic acid dimer. It has been extensively investigated as a model double proton transfer system. Numerous experimental[1-5] and theoretical[6-9] papers on FAD and related systems have been published in recent years.

Early theoretical work on FAD was primarily concerned with its equilibrium geometry and its electronic structure.[6-9] In particular, of the earlier papers, the calculation of Hayashi *et al.*[8] involved a systematic determination of the electronic structure at the SCF-CISD (self-consistent field—singly and doubly excited configuration interaction) level. These authors obtained a value of 12.3 kcal/mol for the classical energy barrier, i.e., the energy difference between the equilibrium geometry and the saddle point on the geometrical potential energy surface.

The minimum energy path (MEP)[10] on the potential energy surface for the double proton transfer of FAD involves a complex set of nuclear displacements (See Sec. III of this paper). Starting at the equilibrium geometry (Fig. 1), the initial motion along the MEP is predominantly heavy atom displacements, bringing the formic acid monomer units closer to each other. Near the barrier (geometrical saddle point on the potential energy surface), the MEP becomes hydrogenic motion as the protons are transferred.

The double proton transfer of FAD is analogous to the well-studied double proton transfer of benzoic acid dimers in the solid state[1(p)] and the intramolecular single proton transfer in gas phase of malonaldehyde.[11-13] In these systems, the proton transfer process is manifested by a tunneling splitting of the ground vibrational state of the system. In fact, a tunneling splitting may also be calculated for certain excited vibrational states for proton transfer reactions of this type.[13]

The first calculation of a tunneling splitting for FAD was reported in 1987 by Chang *et al.*[9] yielding a splitting of $\Delta = 0.3\ cm^{-1}$. They employed a WKB method in analogy to a previous calculation of malonaldehyde.[11] The calculation of the tunneling splitting was based on the assumption that the proton transfer occurs through the geometrical saddle point on the potential energy surface and the proton transfer motion is entirely hydrogenic.

The tunneling splitting of FAD has never been observed experimentally, although some indirect evidence of tunneling has been reported,[1-5] and a rigorous assessment of the theoretical results is not yet feasible. Indeed, new theoretical results on FAD would be helpful to guide experimental work on this problem.

Considering the importance of the double proton transfer of FAD as a key prototype for multiple proton transfer reactions, we recently began a considerably more extensive and more detailed calculation on this system than has been published to date. We chose to employ the reaction surface Hamiltonian framework which has been shown to be an effective method for calculating tunneling splittings for proton

[a] Present address: Division of Theoretical Studies, Institute for Molecular Science, Myodaiji, Okazaki, 444 Japan.
[b] Reprint requests should be sent to either of these authors.

 0021-9606/91/053633-11$03.00

transfer reaction, such as in malonaldehyde.[11-12] Proton transfer reaction between heavy atoms (e.g., oxygen) fall into the heavy–light–heavy category of reaction dynamics. Reaction motion for these systems can deviate strongly from the MEP.[12-17] Many effective procedures have been developed to make tunneling calculations for heavy–light–heavy systems. The reaction surface Hamiltonian approach is well suited to tunneling splitting problems, especially for the calculation of tunneling splitting in excited vibrational states and the determination of vibrational wave functions in proton tunneling reactions. As discussed below, the reaction surface Hamiltonian approaches allow for an explicit treatment of multidimensional vibrational dynamics—albeit at an approximate, reduced dimensionality level.

The reaction surface Hamiltonian method, introduced in 1986 by Carrington and Miller,[12] involves the decomposition of coordinate space into two parts, a reaction surface and a small displacement from the reaction surface, as discussed in Sec. II. Carrington and Miller demonstrated the approach for a calculation of the tunneling splitting of the intramolecular proton transfer of malonaldehyde, as represented by the following:

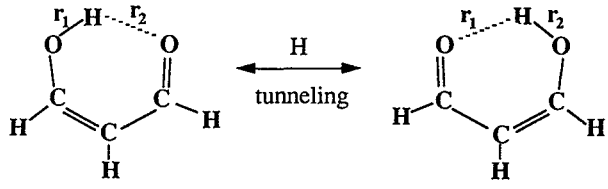

These investigators calculated the tunneling splitting for malonaldehyde by solving an effective nuclear Schrödinger equation, using two independent variables, the O–H bond lengths r_1 and r_2. The remaining degrees of freedom were adjusted to minimize the potential energy part for given sets of (r_1,r_2). The contribution from the adjusted degrees of freedom to the intramolecular proton transfer were included adiabatically, assuming *local normal modes.*

In 1989, we reported a three-dimensional reaction surface Hamiltonian calculation of the tunneling splitting of malonaldehyde that included r_1,r_2 and the intraoxygen separation as the surface variables.[13] The calculated tunneling splitting was ~50% smaller than experiment and the calculated hydrogen/deuterium isotope effect was within 40% of experiment. In addition, tunneling splittings were calculated for excited vibrational states of malonaldehyde. The ground state vibrational wave function of malonaldehyde was analyzed to extract an effective curvilinear tunneling path.

In this paper, we describe a reaction surface Hamiltonian calculation for FAD. One motivation for this work was to estimate the previously unmeasured tunneling splitting for FAD. Eventually, when experimental values are available, the comparison to our theoretical prediction will offer a new test of the accuracy of the reaction surface Hamiltonian method. The results of this paper also offer insight into the multidimensional character of double proton transfer reaction, especially with regard as to whether the double proton transfer reaction involves asynchronous proton motion. Finally, we also explore the role of vibrational excitation in promoting the tunneling processes.

The paper is organized as follows. Section II reviews the basic formulation of the reaction surface Hamiltonian method and describes in detail our theoretical methods including the electronic structure calculations that were used to construct the potential energy surface and the vibrational calculations that were used to determine the tunneling splitting and vibrational wave functions for FAD. Section III describes the results, making comparison where possible to experimental data and previously published theoretical calculations. The paper is summarized in Sec. IV.

II. METHOD OF CALCULATION

A. Summary of reaction surface Hamiltonian method

In this section, we summarize the reaction surface Hamiltonian method which was originally proposed by Carrington and Miller.[12] Our alternative formulation of the procedure is also reviewed.[13]

The essence of the method is that the entire coordinate space $(\mathbf{X})$ is divided into two parts, a reaction surface $[\mathbf{S}(\mathbf{r})]$ and a small displacement $[\mathbf{L}(\mathbf{r})\mathbf{Q}]$ from the reaction surface:

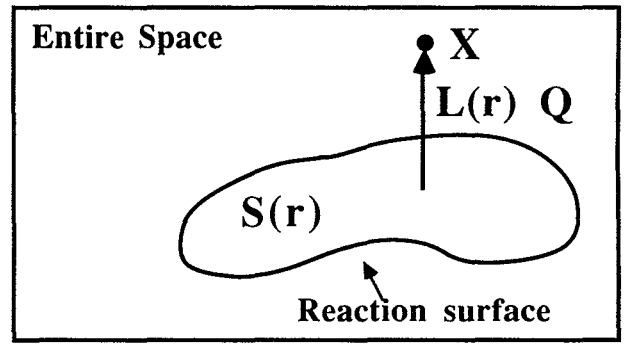

An arbitrary point $\mathbf{X}$ in mass-weighted molecule fixed Cartesian coordinates is related to $\mathbf{S}(\mathbf{r})$ and $\mathbf{L}(\mathbf{r})\mathbf{Q}$ as follows:

$$X_i = S_i(\mathbf{r}) + \sum_{\alpha}^{3N-6-m} L_{i\alpha}(\mathbf{r})Q_\alpha, \tag{2.1a}$$

$$\mathbf{X} = \{\sqrt{\mathbf{m}_1}x_1,\sqrt{\mathbf{m}_1}y_1,\sqrt{\mathbf{m}_1}z_1,\ldots,\sqrt{\mathbf{m}_N}z_N\}, \tag{2.1b}$$

where (x_i,y_i,z_i) is the position of atom i in Cartesian coordinates, N is the number of nuclei, $\mathbf{m}_i$ is the nuclear mass of atom i, and m is the dimensionality of the reaction surface. $\mathbf{r}$ is a reaction surface variable. $\mathbf{S}(\mathbf{r})$ is the reaction surface expressed in terms of mass-weighted Cartesian coordinates. $\mathbf{L}(\mathbf{r})$ transforms small displacements of the bath coordinates to mass-weighted Cartesian coordinates. $\mathbf{Q}$ is a *local normal coordinate.* Ideally, this partitioning should be taken such that $\mathbf{S}(\mathbf{r})$ describes every important reaction path and $\mathbf{L}(\mathbf{r})\mathbf{Q}$ describes only dynamic coupling to the $\mathbf{S}(\mathbf{r})$.

The reaction surface Hamiltonian[12] takes the following form:

$$\hat{H}(\mathbf{r},\mathbf{p}_r,\mathbf{Q},\mathbf{p}_Q) = \tfrac{1}{2}(\mathbf{p}_r^T \mathbf{p}_Q^T)\begin{pmatrix} \mathbf{G}_{rr} & \mathbf{G}_{rQ} \\ \mathbf{G}_{Qr} & \mathbf{G}_{QQ} \end{pmatrix}\begin{pmatrix} \mathbf{p}_r \\ \mathbf{p}_Q \end{pmatrix} + V_0(\mathbf{r}) + \tfrac{1}{2}\sum_{\alpha}^{3N-6-m} \omega_\alpha^2(\mathbf{r}) Q_\alpha^2, \tag{2.2}$$

where $\mathbf{p}_r$ and $\mathbf{p}_Q$ are conjugate momenta of $\mathbf{r}$ and $\mathbf{Q}$. $\mathbf{G}(\mathbf{r})$ is essentially equivalent to the Wilson's G matrix.[18] The explicit form of the G matrix is given in Eq. (2.6) of Ref. 13. $\omega(\mathbf{r})$ can be calculated as Eq. (2.20) of Ref. 13. In Eq. (2.2), the reaction surface is assumed to be the *minimum energy surface*, see below.[12,13]

To construct the minimum energy surface, the following condition must be fulfilled at every surface point;

$$\{1 - \mathscr{P}^{(\mathbf{r})}[\mathbf{S}(\mathbf{r})]\}\mathbf{g}_X[\mathbf{S}(\mathbf{r})] = \mathbf{0}. \tag{2.3}$$

where $\mathbf{g}_x$ is the gradient vector in a mass-weighted Cartesian coordinate system defined as follows:

$$[\mathbf{g}_X(\mathbf{X})]_i = \frac{\partial V(\mathbf{X})}{\partial X_i}. \tag{2.4}$$

$\mathscr{P}^{(\mathbf{r})}$ is the projection operator which projects an arbitrary vector onto the $\mathbf{r}$ space. [The explicit form of the $\mathscr{P}^{(\mathbf{r})}$ is given in Eq. (2.12) of Ref. 13.]

The adiabatic Hamiltonian[12] can be obtained by neglecting the off-diagonal couplings in Eq. (2.2), yielding the following equation:

$$\hat{H}(\mathbf{r},\mathbf{P}_r) = \tfrac{1}{2}\mathbf{P}_r^T \mathbf{G}_{rr}(\mathbf{r})\mathbf{P}_r + V_0(\mathbf{r}) + \tfrac{1}{2}\sum_{\alpha}^{3N-6-m} \bar{\omega}_\alpha(\mathbf{r}). \tag{2.5}$$

$\bar{\omega}$ is obtained by diagonalizing $\mathbf{G}_{QQ}(\mathbf{r})\omega(\mathbf{r})$ as follows:

$$\sum_{\beta}^{3N-6-m} [\mathbf{G}_{QQ}(\mathbf{r})]_{\alpha\beta}\omega_\beta^2(\mathbf{r})\bar{\Lambda}_{\beta\gamma}(\mathbf{r}) = \bar{\omega}_\alpha^2(\mathbf{r})\bar{\Lambda}_{\alpha\gamma}(\mathbf{r}). \tag{2.6}$$

B. Reaction surface of FAD

The adiabatic reaction surface Hamiltonian procedure for calculating vibrational wave functions and tunneling splittings is based on certain approximations with regard to the dynamic coupling of bath and surface variables. The accuracy of the procedure depends on the suitability of the choice of surface coordinates. In previous calculations of tunneling splittings by the reaction surface Hamiltonian method (i.e., for malonaldehyde), the reaction surface coordinates were chosen based upon intuition. An attempt was made to include the internal displacements most obviously coupled to the proton transfer process. For FAD, the choice of surface variables should allow for some of the special features of this double proton transfer reaction, such as the expected importance of the distance between the monomer units on the proton transfer energetics and the possibility that the transfer can be synchronous or asynchronous. The starting point for our choice of a surface coordinate system was the set of six internal coordinates, r_1, r_2, r_3, r_4, R_1, and

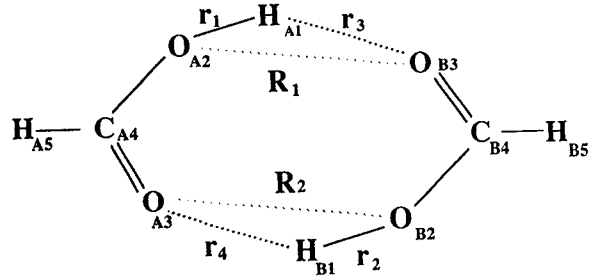

R_2: r_1–r_3 and r_2–r_4 represent the proton movement of $\mathbf{H}_{A1}$ and $\mathbf{H}_{B1}$, respectively, R_1 and R_2 represent the relative motion of the two formic acid monomers. Using these six internal coordinates, we define the following four symmetry adapted coordinates, ρ_1, ρ_2, ρ_3 and ρ_4:

$$\rho_1 = r_1 + r_2 - r_3 - r_4, \tag{2.7a}$$

$$\rho_2 = R_1 + R_2, \tag{2.7b}$$

$$\rho_3 = r_1 - r_2 - r_3 + r_4, \tag{2.7c}$$

$$(\rho_4 = R_1 - R_2). \tag{2.7d}$$

ρ_1 and ρ_3 describe the symmetrized proton movement of $\mathbf{H}_{A1}$ and $\mathbf{H}_{B1}$. The former coordinate represents the symmetric (synchronized) proton movement and the latter represent the asymmetric (nonsynchronized) one. ρ_2 and ρ_4 describe the relative motion of two formic acid monomers. ρ_2 shortens both O–H–O bonds simultaneously, lowering the reaction barrier height to double proton transfer (see below). In contrast, ρ_4 is a wagging motion of two formic acid monomers shortening one O–H–O bond while lengthening the other, making this coordinate less energetically important. Accordingly, we have included ρ_4 in the bath, rather than treating it as a reaction surface variable.

Using ρ_1, ρ_2, and ρ_3 as the reaction surface variables, the minimum energy reaction surface of FAD is defined by optimizing the other geometrical degrees of freedom to minimize the potential energy surface according to Eq. (2.3).

C. Potential energy surface and dynamics calculations

For the calculation of the potential energy surface, we have used the *ab initio* SCF and the *ab initio* MCPF[19] (modified coupled pair functional) methods. The procedure for this calculation which is closely analogous to our previous calculation on malonaldehyde,[13] is summarized as follows;

(1) Constrained geometry optimization and normal vibration analysis was carried out at the SCF level for 76 different points. Each point corresponds to a specific set of values for (ρ_1,ρ_2,ρ_3).

(2) MCPF calculations were carried out in order to get the dynamic electron correlation effect for 26 selected geometry points on the SCF reaction surface.

(3) Analytical expressions for the potential energy surface at the SCF level $[V_0^{\mathrm{SCF}}(\mathbf{r})]$, the correlation energy $[V_0^{\mathrm{cor.}}(\mathbf{r})]$ and the local normal frequencies $[\sum_k^{3N-9} \tfrac{1}{2}\omega_k^{\mathrm{SCF}}(\mathbf{r})]$ on the reaction surface were obtained by a least square fitting procedure.

The final potential energy surface, including the zero-point energy correction, is expressed as

$$V(\mathbf{r}) = V_0^{\mathrm{SCF}}(\mathbf{r}) + V_0^{\mathrm{cor.}}(\mathbf{r}) + \sum_{k}^{3N-9} \tfrac{1}{2}\omega_k^{\mathrm{SCF}}(\mathbf{r}). \quad (2.8)$$

The basis sets used in the SCF calculation were of MIDI4[20] (split valence) quality augmented by p type polarization functions (orbital exponent, $\alpha = 0.68$) on the moving two protons. In the MCPF calculation, Duijneveldt's $(7s4p)$, $(7s4p)$, $(4s)$ basis sets were used on O, C, and H, respectively.[21] p type polarization functions ($\alpha = 1.00$) on the moving protons and d type polarization functions ($\alpha = 0.85$) on O were also added to these basis sets. These basis sets were contracted to $[4s2p1d]$, $[4s2p]$, $[2s(1p)]$, respectively, employing the general contraction scheme[22] using atomic SCF orbitals.

Vibrational eigenstates using the reaction surface Hamiltonian were obtained in the vibrational MCSCF calculations. Further details are given in Ref. 29(c).

The SIRIUS,[23] ABACUS,[24] MOLECULE/SWEDEN,[25] and VIBRA[26] program systems were used for the constrained optimizations/normal vibrational analyses, the MCPF calculations and the vibrational MCSCF calculations, respectively.

III. RESULTS AND DISCUSSIONS

A. Reaction surface and barrier energy

The potential energy surface of FAD is portrayed in Fig. 2 as a function of ρ_1 and ρ_2. The equilibrium geometries (EQ) have a larger spacing between the monomers (ρ_2) than the saddle point geometry (A), which lies on the $\rho_1 = 0$ line by symmetry. Figure 1 gives a qualitative picture of the geometry changes associated with the EQ→A (saddle point) displacement. Note that contours are not shown in Fig. 2 for regions of the surface where the energy exceeds 0.045 a.u. above the energy of the equilibrium geometry.

Figure 2 was constructed with ρ_3 (the asynchronous proton motion) fixed at ($\rho_3 = 0$). In fact, $\rho_3 = 0$ does not in general correspond to a minimum energy. This is demonstrated in Fig. 3, where the potential energy is plotted for three different sets of fixed ρ_1 and ρ_2 values A, B, and C, lying on the $\rho = 0$ ridge between the "product" and "reactant" valleys. The letters correspond to points in Fig. 2. Note that for A and B, a single minimum in the energy dependence of ρ_3 is observed at $\rho_3 = 0$. At these two points on the potential

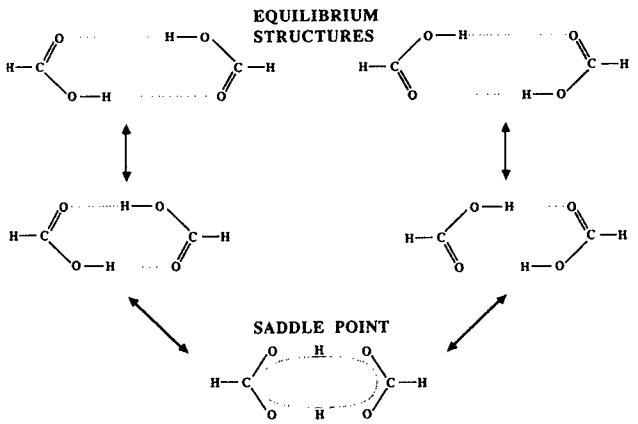

FIG. 1. A schematic representation of the double proton transfer process in formic acid dimer along the classical reaction path.

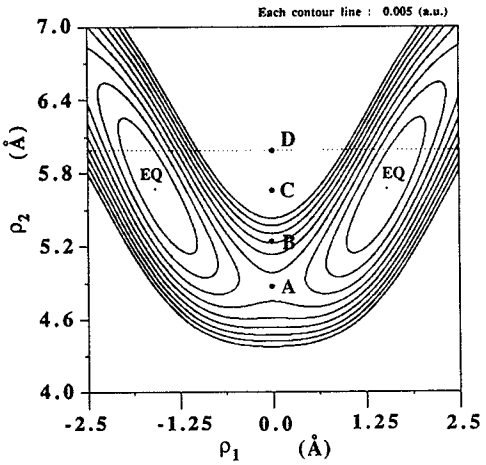

FIG. 2. A plot of the potential energy surface on the reaction surface, $V(\rho)$ in Eq. (2.8). The missing variable ρ_3 in the figure is fixed at 0.0. Four points, A, B, and C, D in the figure are described in the text.

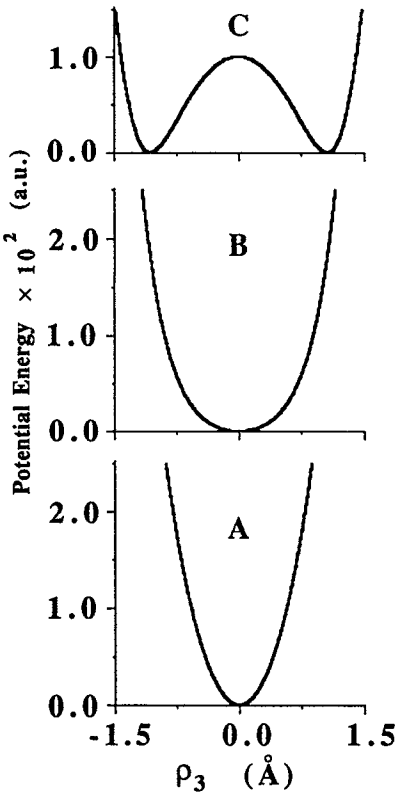

FIG. 3. Plots of the potential energies on the reaction surface, $V(\rho)$ in Eq. (2.8) along ρ_3 for three fixed sets of (ρ_1,ρ_2) values. These three sets of (ρ_1,ρ_2) are shown as the points, A, B, and C in Fig. 2.

energy surface, *at most one single negative eigenvalue exists for the Hessian* $\partial^2 V(\rho)/\partial\rho^2$, i.e., along the ρ_1 direction. In contrast, at C in Fig. 3 V shows two minima, such that the Hessian matrix has *two negative eigenvalues* around $\rho_1 = 0$ and $\rho_3 = 0$, i.e., one along ρ_1 and one along ρ_3. In mathematical terms, for point C the following condition is satisfied:

$$\left(\frac{\partial^2 V(\rho)}{\partial\rho_3^2}\right)_{\substack{\rho_1=\rho_1 \\ \rho_2=\rho_2 \\ \rho_3=0}} = 0. \tag{3.1}$$

This signifies that at points C, the double proton transfer motion may be bifurcated into two equivalent paths in the *full three-dimensional* (ρ_1, ρ_2, *and* ρ_3) *surface*. This is more clearly demonstrated if we examine a contour plot of the potential energy surface as a function of the symmetric coordinate ρ_1 and the asymmetric proton coordinate ρ_3 with fixed inter-monomer displacement coordinate ρ_2. Figure 4 shows a plot of this type with $\rho_2 = 6.0(\text{Å})$. Note that this surface includes D in Fig. 2. In fact, the geometries that lie on a horizontal line passing through D on Fig. 2, correspond to the geometries that fall on a horizontal line bisecting Fig. 4. In Fig. 4, we show a MEP in the (ρ_1,ρ_3) coordinate space for $\rho_2 = 6.0(\text{Å})$. Note that the path has two equivalent saddle points separating the minimum energy points. Furthermore, the maximum point (D) has two negative eigenvalues as described above. Each path corresponds to asynchronous motion of the two protons, in the sense that ρ_3 is not equal to zero at every point along the path.

This bifurcation only occurs when $\partial^2 V(\rho)/\partial\rho_3^2$ is negative. The regions where this is the case are indicated in Fig. 5 by the dark areas. Note that C and D fall into a dark area, but A and B do not, see Fig. 2. The dark pattern area arises when $|\rho_1|$ becomes small and ρ_2 becomes large, or when $|\rho_1|$ becomes large and ρ_2 becomes small. (See the position of the dark pattern in Fig. 5.) The asymptotic geometries of these

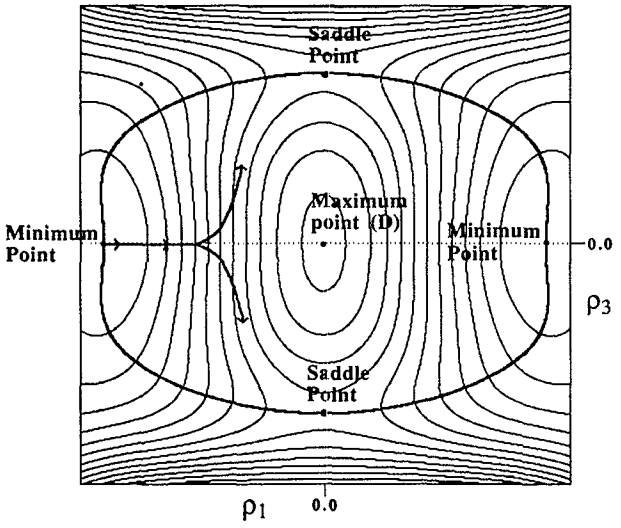

FIG. 4. A sketch of the potential energy surface for the asynchronous proton transfer process in formic acid dimer. The solid circle line in the figure passing through the minimum energy points and the saddle points is the minimum energy path. See the text for further detail.

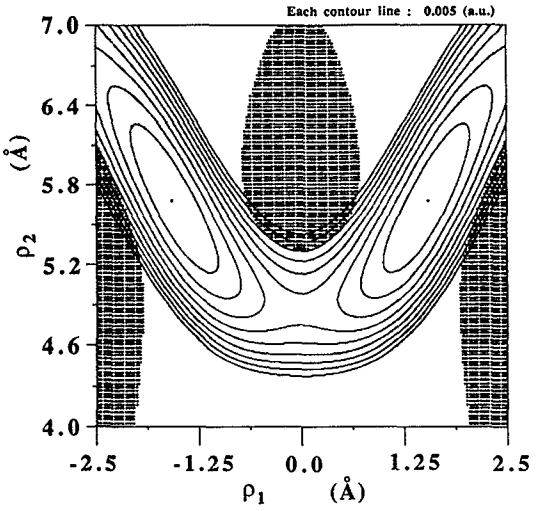

FIG. 5. A plot of the potential energy surface on the reaction surface, $V(\rho)$ in Eq. (2.8). The axis system is same as that of the Fig. 2. The variable ρ_3 in the figure is fixed at 0.0. The dark pattern represents the area where the second derivative of $V(\rho)$ with respect to ρ_3 is negative.

correspond to the high energy exit channels (dissociation). The lowest energy exit channel (i.e., FAD dissociating into two formic acid monomers) lies on the direction where both $|\rho_1|$ and ρ_2 become large.

The bare potential energies (without the zero-point energy correction) at the SCF and the MCPF levels are plotted in Figs. 6 and 7, respectively. In these figures ρ_3 is set equal to zero. The inclusion of electron correlation effects lowers the reaction barrier—{(saddle point energy) − (equilibrium geometry)}—and changes the equilibrium geometries. It also significantly alters the shape of the potential energy surface.

The total energies at the equilibrium structures and the saddle point are given in Table I, together with those of previous work. The reaction barrier of 16.5 kcal/mol at the SCF level agrees well with the previous SCF prediction of 15.6

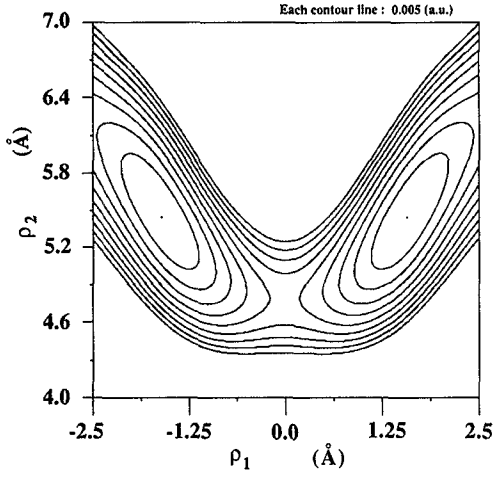

FIG. 6. A plot of the reaction surface, $V_0^{\text{SCF}}(\rho)$ in Eq. (2.8). The variable ρ_3 in the figure is fixed at 0.0.

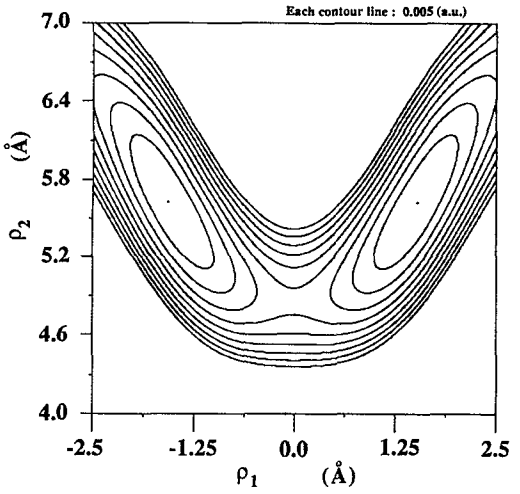

FIG. 7. A plot of the reaction surface, $[V_0^{SCF}(\rho) + V_0^{Cor}(\rho)]$ in Eq. (2.8). The variable ρ_3 in the figure is fixed at 0.0.

kcal/mol by Chang *et al.*[9] Our MCPF prediction of 12.0 kcal/mol is very close to the single reference CISD prediction (12.3 kcal/mol) by Hayashi *et al.*[8] However, it should be noted that the geometries in both these correlated calculations are not fully optimized. The calculations of Hayashi *et al.* employed SCF optimized equilibrium and saddle point geometries for the CISD calculation of the barrier energy. In contrast, our calculation of the barrier energy is directly from our analytical expression for the potential energy surface. Thus, the MCPF correction of the SCF level calculation, in our case, corrects the energies, and to some extent, the MCPF calculation also alters the geometries of the equilibrium and saddle points (see Fig. 8).

B. Basis set dependence and higher order dynamic correlation

In order to evaluate the accuracy of our *ab initio* calculation of the potential energy surface, we have made benchmark calculations of the barrier energy for various basis sets. The results are summarized in Table II. The basis sets are summarized in Table III. For all of these calculations, the same equilibrium and saddle point geometries were used. These geometries were optimized at the SCF level with the basis set III (MIDI-4).

TABLE I. A comparison of various calculations of the total energy and the proton transfer barrier for formic acid dimer.

Method	Total energy (a.u.)	Barrier height (kcal/mol)	Basis set
This work			
SCF	− 376.987 662	16.5	III[a]
MCPF	− 378.140 971	12.0	IV[a]
Previous work			
SCF(Ref. 9)	− 377.651 6	15.6	(DZ + P)
CI-SD(Ref. 8)	− 377.556 8	12.3	(4-31G)

[a] See Table III.

TABLE II. Calculated total energies and barrier heights from various calculational schemes and different basis sets. The basis sets used are summarized in Table III.

Method	Total energy (a.u.)	Barrier height (kcal/mol)	Basis set[a]
SCF	− 377.705 221	17.4	I
CI_{SD}	− 378.614 770	12.4	I
$CI_{SD(Q)}$	− 378.790 858	10.8	I
MCPF	− 378.828 989	10.1	I
SCF	− 377.210 790	16.4	II
MCPF	− 378.137 351	9.3	II
SCF	− 376.987 662	16.5	III

[a] See Table III.

The best SCF prediction with the large basis set, I gives a reaction barrier of 17.4 kcal/mol. The smaller basis sets, II and III, give 16.4 and 16.5 kcal/mol, respectively. Even with the smallest basis set III (MIDI-4), the difference of the reaction barrier from the best SCF prediction is at most 1 kcal/mol.

The single reference CISD calculation lowers the barrier height to 12.4 kcal/mol. (The weight of the SCF configuration at the two geometries are larger than 0.9, and no other important electron configurational state is found for the reference state.) The effect of the quadruple excitations estimated from Davidson's correction[27] with basis set I further lowers the barrier height to 10.8 kcal/mol [CISD(Q)], which is very close to the 10.1 kcal/mol of the MCPF prediction. The method we employed to calculate the potential energy surface, a MCPF calculation with basis II, gives reaction barrier of 9.3 kcal/mol.

C. Geometries

We have determined the equilibrium and saddle point geometries at the SCF and the MCPF levels of theory. These geometries are shown in Fig. 8, together with the experimental prediction.[2] We mention again that the predicted geometries at the MCPF are not completely optimized, as discussed above.

TABLE III. The basis sets used for the calculations in Tables I and II.

	I[a]	II[a]	III[b]	IV[a]
P (tunneling protons)	[3*s*2*p*] (6*s*2*p*)	[2*s*1*p*] (4*s*1*p*)	[2*s*1*p*] (4*s*1*p*)	[2*s*1*p*] (4*s*1*p*)
O	[4*s*3*p*2*d*] (11*s*6*p*2*d*)	[3*s*2*p*1*d*] (7*s*4*p*1*d*)	[3*s*2*p*] (7*s*4*p*)	[4*s*2*p*1*d*] (7*s*4*p*1*d*)
C	[4*s*3*p*1*d*] (11*s*6*p*1*d*)	[3*s*2*p*] (7*s*4*p*)	[3*s*2*p*] (7*s*4*p*)	[4*s*2*p*] (7*s*4*p*)
H	[3*s*1*p*] (6*s*1*p*)	[2*s*] (4*s*)	[2*s*] (4*s*)	[2*s*] (4*s*)

[a] van Duijneveldt *et al.* (Ref. 21).
[b] MIDI-4···Tatewaki *et al.* (Ref. 20).

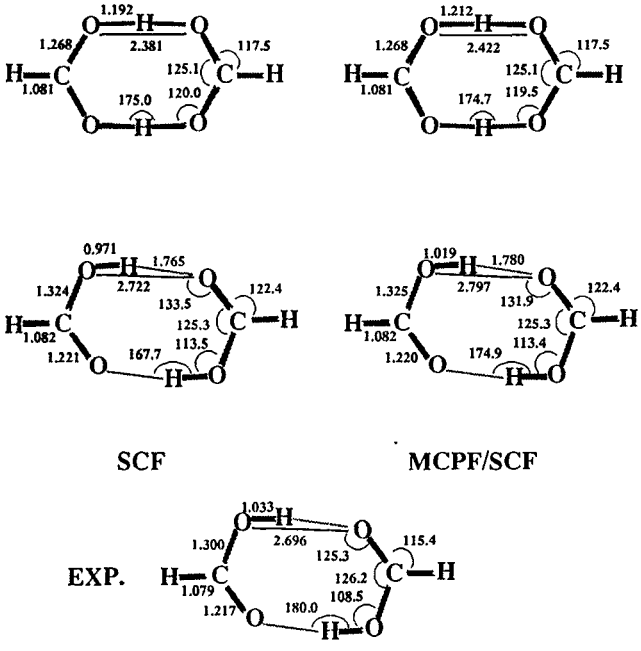

FIG. 8. The equilibrium and the saddle point geometries of formic acid dimer at the SCF and the MCPF/SCF levels. EXP. is the experimental prediction of the equilibrium structure (Ref. 2).

When electron correlation effects are included, the O–H, the H···O and the O···O distances and the ∠(H···O–C) and the ∠(O–H···O) angles are significantly altered from the SCF predictions (see Fig. 8). The correlated values are closer to the experimental values. An exception is the O···O distance.

D. Formic acid monomer and dimerization energy

We have also calculated the total energy and the equilibrium geometry of formic acid monomer (FA) in order to further test the reliability of our calculational scheme. The equivalent calculational scheme to that of FAD was employed for these calculations;

(1) The O–H distance was chosen as the reaction surface variable.

(2) The one-dimensional minimum energy surface was calculated at the SCF level.

(3) MCPF calculations were carried out in order to make corrections for the correlation effect.

(4) The equilibrium geometry and the total energy were determined from the analytical expression of the one dimensional potential energy surface.

The predicted equilibrium geometry is shown in Fig. 9, together with the experimental prediction.[3] At the MCPF geometry, the O–H distance is remarkably altered from the SCF prediction and is closer to the experimental value.

The dimerization energy of FA (the dissociation energy for the lowest energy exit channel in FAD) (D_e) is shown in Table IV, together with the three experimental values.[4] The 13.9 kcal/mol of the D_e in the MCPF prediction falls in the range of the experimental values.

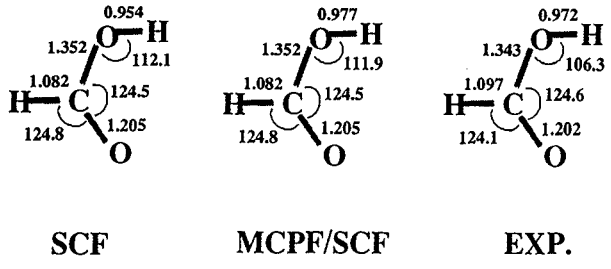

FIG. 9. The equilibrium and the saddle point geometries of formic acid monomer at the SCF and the MCPF/SCF levels. EXP. is the experimental prediction of the equilibrium structure (Ref. 3).

E. Ground state tunneling splittings

We have calculated the frequencies and eigenfunctions of the lowest 16 vibrational states of the reaction surface. The frequency difference between the two lowest states (0.004 cm^{-1}) corresponds to the tunneling splitting of the ground vibrational state. The splitting for excited vibrational states will be discussed later. Table V compares the calculated tunneling splitting, and other properties, from this work with a previous calculation by Chang *et al.*[9] The previous calculation differs in several respects which seem to account for much larger tunneling splitting. A significantly larger barrier (15.8 kcal/mol), calculated at the SCF level, was used in the calculation by Chang *et al.* But, more significantly, the previous calculation employed a simple WKB model, in which the reaction coordinate was assumed to be well approximated by pure O–H stretching motion, and the effective barrier energy was still assumed to be the barrier energy of the saddle point. Our calculations reveal that the tunneling path (see below) deviates so significantly from the region of the saddle point, that a much larger effective barrier applies to this reaction. Our results suggest that the simple WKB model is not appropriate for FAD.

F. Normal vibrations and excited vibrational states

The normal vibrational analysis at the equilibrium geometry of FAD is shown in Table VI, together with the subspace normal frequencies (ω_s) at the same equilibrium geometry. The ω_s is defined as follows:

$$\mathscr{P}^{(r)}(\mathbf{X})\mathbf{H}(\mathbf{X})\mathscr{P}^{(r)}(\mathbf{X})\mathbf{L}_s(\mathbf{X}) = \mathbf{L}_s(\mathbf{X})\omega_s^2(\mathbf{X}), \quad (3.2)$$

TABLE IV. A comparison of various calculated values of the dimerization energy for formic acid (kcal/mol).

	SCF	MCPF	EXP.
D_0	19.1	16.2	···
Zero-point energy correction	−2.3	−2.3[d]	···
D_e	16.8	13.9	14.8 ± 0.5[a] 14.1 ± 0.1[b] 11.7 ± 0.1[c]

[a] Ciague *et al.* [Ref. 4(a)].
[b] Mathews *et al.* [Ref. 4(b)].
[c] Henderson [Ref. 4(c)].
[d] The zero-point energy correction was taken from the SCF calculation.

TABLE V. The tunneling splitting of the ground vibrational state and the effective barrier height for formic acid dimer.

	This work	Previous work[a]
Tunneling splitting (cm^{-1})	0.004	0.3
Effective barrier height (kcal/mol)	11.8	15.8
Bare barrier height (kcal/mol)	12.0	15.6
Zero-point energy correction (kcal/mol)	−0.2	0.2

[a] Chang *et al.* (Ref. 9).

where $\mathbf{H}(\mathbf{X})$ is the nuclear Hessian matrix (with the rotational and the translational components already projected out in mass-weighted Cartesian coordinates) and $\mathscr{P}^{(r)}(\mathbf{X})$ is the projection operator which projects an arbitrary vector onto r space (See Sec. II). The three ω_s values corresponds to the normal frequencies on the reaction surface.

The two ω_s with high frequencies (3674 and 3683 cm^{-1}) have nearly exact correspondence with the two highest frequency modes in the full space. (The overlaps between the modes are 0.99 and 0.97, cf. Table VI.) These two modes are the symmetric (A_g) and the asymmetric (B_u) O–H stretching modes. The remaining mode ($\omega_s = 767$ cm^{-1}) has significant overlap with several normal modes of A_g symmetry in the full space. However, the main component of the $\omega_s = 767$ cm^{-1} mode is the intermonomer stretch, consistent with our choice of ρ_2 as a surface variable.

As stated above, we have calculated the frequencies and eigenfunctions for the lowest 16 vibrational states of the reaction surface. The levels fall into 8 pairs whose average frequencies (transition energy) and splittings are summarized in Table VII. The levels can be straightforwardly assigned to overtones and combination levels of the harmonic modes of the subspace. The vibrational spacings are nearly perfectly harmonic.

The proton tunneling splitting dramatically increases as successive quanta are added to mode 1, which corresponds to large amplitude relative motion of the monomer units. We observed an analogous enhancement of the tunneling splitting of malonaldehyde where the O–O stretching vibration was excited.[13,28] For FAD, the tunneling splitting presumably increases (in simple terms) because as mode 1 is excited, the root mean square amplitude of the heavy atom motion increases. Thus, there is a larger probability of smaller ρ_2 values, i.e., where proton tunneling is more effective. In contrast, vibrational excitation of mode 2 (primarily asymmetric proton stretch) does not increase the vibrational amplitude in the region of the surface where tunneling is favored. In fact, excitation of mode 2 actually reduces the tunneling splitting.

TABLE VI. Vibrational normal modes at the SCF level for the formic acid dimer. The relationship between normal modes of the subspace and the full-space are indicated by arrows. The numerical value associated with each arrow is the magnitude of the vibrational overlap of the pair of modes connected by the arrow. See the text for further detail.

Subspace (cm^{-1})	Overlap	Full space (cm^{-1})	Character
A_g			
		177	CO_{A2}–H_{A1}–O_{B3}, O_{B2}–H_{B1}–O_{A3} bend
	0.84→	207	Inter-monomer stretch
	0.30→	700	O_{A2}–C_{A4}–O_{A3}, O_{B2}–C_{B4}–O_{B3} bend
	0.26→	1291	O_{A2}–C_{A4}, O_{B2}–C_{B4} stretch
767	0.25→	1499	C_{A4}–O_{A2}–H_{A1}, C_{B4}–O_{B2}–H_{B1} bend
		1539	O_{A2}–C_{A4}–H_{A5}, O_{B2}–C_{B4}–H_{B5} bend
	0.27→	1817	O_{A3}–C_{A4}, O_{B3}–C_{B4} stretch
		3380	C_{A4}–H_{A5}, C_{B4}–H_{B5} stretch
3674	→	3705	O_{A2}–H_{A1}, O_{B2}–H_{B1} stretch
	0.99		
B_u			
		255	O_{A2}–O_{B3}, O_{B2}–O_{A3} stretch
		1289	O_{A2}–C_{A4}, O_{B2}–C_{B4} stretch
		1476	C_{A4}–O_{A2}–H_{A1}, C_{B4}–O_{B2}–H_{B1} bend
		1534	O_{A2}–C_{A4}–H_{A5}, O_{B2}–C_{B4}–H_{B5} bend
		1861	O_{A3}–C_{A4}, O_{B3}–C_{B4} stretch
		3378	C_{A4}–H_{A5}, C_{B4}–H_{B5} stretch
3683	→	3770	O_{A2}–H_{A1}, O_{B2}–H_{B1} stretch
	0.97		
B_g			
		254	C_{A4}–O_{A2}–H_{A1}, C_{B4}–O_{B2}–H_{B1} bend
(out-of-plane mode)		963	O_{A2}–H_{A1}, O_{B2}–H_{B1} bend
		1175	C_{A4}–H_{A5}, C_{B4}–H_{B5} bend
A_u			
		90	twist about C_{A4}–H_{A5}, C_{B4}–H_{B5}
(out-of-plane mode)		180	O_{A2}–H_{A1}–O_{B3}, O_{B2}–H_{B1}–O_{A3} bend
		1005	O_{A2}–H_{A1}, O_{B2}–H_{B1} bend
		1181	C_{A4}–H_{A5}, C_{B4}–H_{B5} bend

G. Tunneling path

We have extracted the effective proton tunneling path from the lowest vibrational eigenfunction of the reaction surface Hamiltonian. For this purpose, we first define orthonormalized, mass-weighted coordinates (q_1, q_2, and q_3) as the surface variables (The detail of these coordinates is described in Appendix 3 in Ref. 13). The potential energy surface in this coordinate system is shown in Fig. 10. q_1, q_2, and q_3 correspond to the original internal coordinates, ρ_1, ρ_2, and ρ_3, respectively, with mass scaling factors. The significance of the dark pattern in Fig. 10 is analogous to Fig. 5. In this area, the second derivative of the potential energy surface with respect to q_3 is always negative.

The MEP line in Fig. 10 is the minimum energy path (steepest descent path from the geometrical saddle point) in

TABLE VII. A list of the excited vibrational energies and the corresponding tunneling splitting on the reaction surface.

Quantum No. ν_1	Quantum No. ν_2	Transition energy (cm^{-1})	Splitting (cm^{-1})
0	0	0	0.004
1	0	241	0.027
2	0	481	0.112
3	0	719	0.339
0	1	605	0.002
1	1	867	0.011
2	1	1128	0.043
3	1	1386	0.127

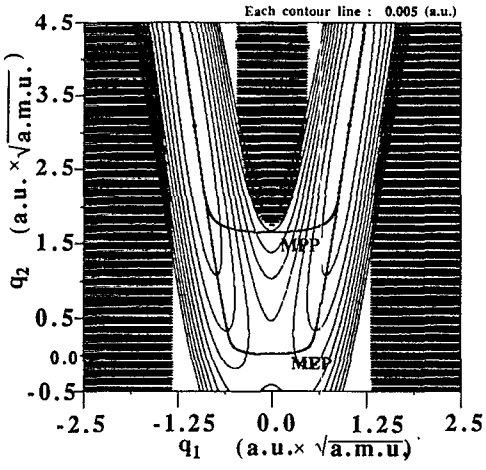

FIG. 10. A presentation of the potential energy surface, $V(\rho)$ in Eq. (2.8), plotted in a mass weighted coordinate system, employing the new variables, q. See the text for further detail about the coordinate system and the two reaction paths, MEP and MPP.

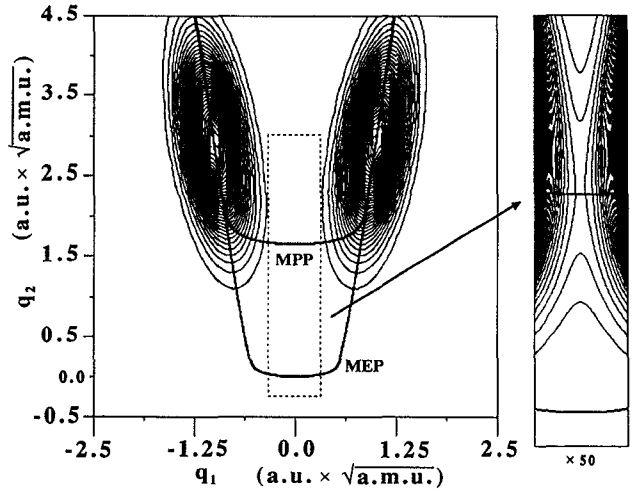

FIG. 11. A plot of contours of the lowest eigenfunction of the reaction surface Hamiltonian. The axis system and the two reaction paths are identical to Fig. 10. Equal spacing in arbitrary units was used for the contour plot. The contour plot in the right side is an expansion of the dotted region in the main figure. The contour spacing in the expanded region is 50 times smaller than the spacing for the main figure, see text for further detail.

the q coordinates. Note that the minimum energy path can not be defined for the portion of the potential energy surface in the exit channels. We have used the gradient extremal criterion for this region of the minimum energy path.[29]

MPP in Fig. 10 is the most probable reaction path between the two equilibrium structures. We suggest the term *maximal probability path* for this reaction path. The MPP is defined as *a steepest descent path of the negative probability distribution function for the vibrational ground state,* $-|\Phi(\mathbf{q})|^2$. The steepest descent path starts at the saddle point and descends to the point of largest nuclear probability (i.e., the reactant or the product). For the MPP in the exit channels, we have used the gradient extremal path for the MPP calculation, as described above for the MEP. (More detail about the MPP concept will be discussed in a forthcoming article.)

In Fig. 11, the MPP, the MEP and the ground vibrational wave function are plotted in the same axis system as Fig. 10. From Fig. 11, one can see that little amplitude of the vibrational wave function is found near the geometrical saddle point (the midpoint of the MEP). It is clear that the MEP criterion, starting from the geometrical saddle point is not an appropriate criterion to define the tunneling path of FAD.

The initial direction of the MPP from the reactant (i.e., one of the equilibrium geometries) is virtually identical to that of the MEP. This initial direction is interpreted as the relative motion of two monomers which is mainly described by q_2. However, the MPP quickly changes its character to hydrogenic motion described by q_1 and shortcuts the MEP, even though the reaction barrier of the MPP is about twice as high as for the MEP (see Fig. 10). This behavior is consistent with the previous conventional picture of heavy–light–heavy mass combination systems.[30]

Around the midpoint of the reaction, the MPP grazes the dark pattern in Fig. 10, indicating the potential involvement of the asymmetric proton movement. We have calculated the tunneling splitting with $q_3 = 0.0$ (frozen) and have found that the splitting decreases by 20%. From this it is reasonable to assume that there is a certain probability for nonsynchronized proton movement, but that it is not an essential element of the reaction. However, the absolute value of the calculated tunneling splitting is very small (0.004 cm^{-1}), so small changes in the potential energy surface may alter this conclusion.

H. Assessment of our reaction surface

Finally, we will assess our choice of the reaction surface. We have employed minimum energy surface criteria to construct the reaction surface, using symmetry adapted internal coordinates as the surface variables. These coordinates were chosen such that ρ_1 represents the symmetric O–H stretching motion, ρ_2 represents the relative motion of two formic acids and ρ_3 represents the asymmetric O–H stretching motion. However, this assignment is not always true in the whole region of the reaction surface, since we have used the displacement coordinates (ρ_1 and ρ_3), not the bond distances themselves. When bond distances become shorter than their equilibrium values, the potential energy increases rapidly, in general. Since ρ_1 and ρ_3 have more freedom than the pure bond distances, no bond distance becomes shorter than its equilibrium value, even if ρ_1 and ρ_3 take any values.

Figure 12 shows the six asymptotic geometries of FAD on the reaction surface. When ρ_2 is inappropriately small compared with ρ_1 or ρ_3, the molecule does not keep a planar structure, and ρ_1 or ρ_3 change characters to out-of-plane bending motion instead of being normal O–H stretching motions. This situation is clearly demonstrated in the geometries, **A**, **B**, **C**, and **D** of Fig. 12. The geometry, **F**, is the normal route to the lowest energy exit channel where two formic acid come apart monomers. The geometry, **E**, is also on the way to this exit channel. However, one of the hydro-

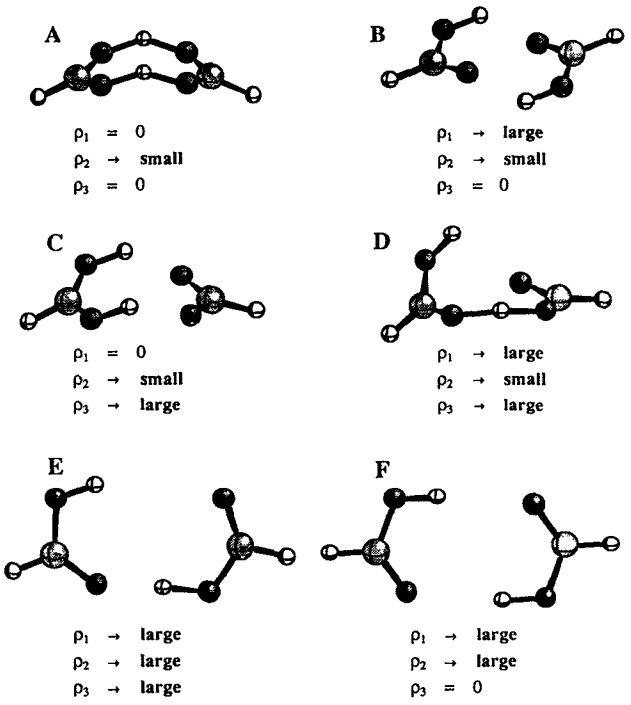

FIG. 12. Six asymptotic geometries of formic acid dimer on the reaction surface. The corresponding ρ values of the six geometries are as follows (unit: Å): A: $\rho_1 = 0.0$, $\rho_2 = 0.0$, $\rho_3 = 4.0$; B: $\rho_1 = -1.2$, $\rho_2 = 0.0$, $\rho_3 = 4.5$; C: $\rho_1 = 0.0$, $\rho_2 = -1.0$, $\rho_3 = 4.5$; D: $\rho_1 = -1.2$, $\rho_2 = -1.0$, $\rho_3 = 4.5$; E: $\rho_1 = -2.5$, $\rho_2 = -1.5$, $\rho_3 = 6.5$; F: $\rho_1 = -2.5$, $\rho_2 = 0.0$, $\rho_3 = 6.5$.

gen bonds breaks completely at first in this route, which has ρ_3 constrained to be large.

As seen in Fig. 12, our coordinate system includes motions other than the pure stretching motions. Table VIII shows the normal frequencies on the reaction surface at the SCF and the MCPF levels. The main characters of the normal modes are symmetric O–H stretch, asymmetric O–H stretch, and O–O stretch, respectively. These frequencies roughly correspond to the subspace frequencies in Table VI. The difference of the frequencies is due to the choice of the coordinate systems; the frequencies in Table VII are obtained by Wilson's GF matrix method[18] in the ρ space. In contrast, those in Table VI refer to mass-weighted Cartesian coordinates. Since the ρ coordinates include various complex motions, the frequencies in Table VI and Table VII are significantly different.

TABLE VIII. Normal frequencies on the reaction surface by Wilson's GF matrix method. See the text for further detail.

MCPF with adiabatic correction (cm^{-1})	SCF with no adiabatic correction (cm^{-1})
$\omega_1 = 3087$	$\omega_1 = 2631$
$\omega_2 = 1410$	$\omega_2 = 1062$
$\omega_3 = 245$	$\omega_3 = 290$

Due to the use of displacement coordinates, ρ and the minimum energy surface criterion, our reaction surface is somewhat different from our initial expectations. However, this situation occurs only in asymptotic regions, not around the important region for the tunneling.

IV. SUMMARY, CONCLUSION, AND FUTURE STUDIES

The double proton transfer reaction of FAD has been investigated within the reaction surface Hamiltonian framework. A three-dimensional reaction surface has been calculated at a high level of *ab initio* accuracy. The calculated tunneling splitting is 0.004 cm^{-1}, which is considerably smaller than the previous theoretical prediction which was based on a simple WKB method. The effective tunneling path (maximal probability path: MPP) on the reaction surface has been extracted from the lowest eigenfunction of the reaction surface Hamiltonian. The MPP deviates dramatically from the minimum energy path on the reaction surface. Our vibrational calculation shows some important evidence for the asymmetric proton movement around the midpoint of the reaction. Various other properties of FAD and the aspects of the reaction surface Hamiltonian method have been investigated and examined.

We have reaffirmed that the reaction surface Hamiltonian method is a practical way to model chemical reactions, when the classical reaction path gives a poor description. In our present work, we have successfully used the minimum energy surface criterion to construct a reaction surface for FAD, using symmetry adapted internal coordinates as the surface variables.

ACKNOWLEDGMENTS

This work was supported by the National Science Foundation (Grant Nos. CHE-8251158 and CHE-8915629), the Petroleum Research Foundation (Grant No. 20288-AC6), and by the Minnesota Supercomputer Institute. The calculations were carried out on Cray-2 and Cray X-MP computers at the Minnesota Supercomputer Center.

[1](a) G. H. Carlson, R. E. Witkowski, and W. G. Fateley, Spectrochim. Acta **22**, 1117 (1966); (b) R. J. Jakobsen, Y. Mikawa, and J. W. Brasch, *ibid.* **23**, 2199 (1967); (c) R. J. Jakobsen, J. W. Brasch, and Y. Mikawa, Appl. Spectrosc. **22**, 641 (1968); (d) A. D. Clague and A. Novak, J. Mol. Struct. **5**, 149 (1970); (e) P. Excoffon and Y. Marechal, Spectrochim. Acta A **28**, 269 (1972); (f) S. Hayashi and J. Uemura J. Chem. Phys. **60**, 2630 (1974); (g) W. G. Rothchild, *ibid.* **61**, 3422 (1974); (h) S. Hayashi and J. Uemura, *ibid.* **63**, 1733 (1975); (i) J. Uemura, J. Mol. Struct. **36**, 35 (1977); (j) J. Chem. Phys. **68**, 42 (1978); (k) S. Tomoda, Y. Achiba, K. Nomoto, K. Sato, and K. Kimura, Chem. Phys. **74**, 113 (1983); (l) B. M. Landsberg, D. Crocker, and R. J. Butcher, J. Mol. Spectrosc. **92**, 67 (1982); (m) J. E. Bertie and K. Michaelian, J. Chem. Phys. **76**, 886 (1982); (n) K. I. Lazaar and S. H. Bauer, J. Am. Chem. Soc. **107**, 3769 (1985); (o) J. E. Bertie, K. Machaelian, H. H. Eysel, and D. Hager, J. Chem. Phys. **85**, 4779 (1986); (p) C. Rambaud, A. Oppeländer, M. Piecce, H. P. Trommsdorff, and J. C. Vial, Chem. Phys. **136**, 335 (1989).
[2]A. Almenningen, O. Bastiansen, and T. Motzfeldt, Acta Chem. Scand. **23**, 2848 (1969) and **24**, 747 (1970).
[3]M. D. Harmony, V. W. Laurie, R. L. Kuczkowski, R. H. Schwendeman, D. A. Ramsay, F. J. Lovas, W. J. Lafferty, and A. G. Maki, J. Phys. Chem. **8**, 619 (1979).

[4](a) A. D. Clague and H. J. Bernstein, Spectrochim. Acta A **25**, 593 (1969); (b) D. M. Mathews and R. W. Sheets, J. Chem. Soc. A **1969**, 2203; (c) G. J. Henderson, Chem. Educ. **64**, 88 (1987).
[5]P. Excoffon and Y. Maréchal, Chem. Phys. **5**, 367 (1974).
[6]G. N. Robertson and M. C. Lawrence, Chem. Phys. **62**, 131 (1981).
[7](a) S. Nishida and K. Nakamoto, J. Chem. Phys. **41**, 1558 (1964); (b) P. Bosi, G. Zerbi, and E. Clementi, *ibid.* **66**, 3376 (1977); (c) S. Yamabe, K. Kitaura, and K. Nishimoto, Theoret. Chim. Acta **47**, 111 (1978); (d) J. L. Derissen and P. H. Smit, Acta Crystallogr. A **34**, 842 (1978); (e) P. H. Smit, J. L. Derissen, and F. B. Duijneveldt, Mol. Phys. **37**, 501 (1979); (f) S. Scheiner and C. W. Kern, J. Am. Chem. Soc. **101**, 4081 (1979); (g) S. Hashimoto, S. Ikuta, and M. Imamura, Chem. Phys. Lett. **62**, 567 (1979); (h) J. Gready, Chem. Phys. **55**, 1 (1981); (i) J. Gready, G. B. Bacskay, and N. S. Hush, *ibid.* **64**, 1 (1982); (j) A. Karpfen, *ibid.* **88**, 415 (1984); (k) N. Ray, M. Shibata, G. Bolis, and R. Rein, Int. J. Quantum Chem. **27**, 427 (1985); (l) C. Mijoule, M. Allavena, J. M. Leclercq, and Y. Bouteiller, Chem. Phys. **107**, 207 (1986); (m) M. J. Wójcik, A. Y. Hirakawa, and M. Tsuboi, Int. J. Quantum Chem. Quantum Biol. Symp. **13**, 133 (1986); (n) R. Meyer and R. R. Ernst, J. Chem. Phys. **86**, 784 (1987); (o) J. Dybal, T. C. Cheam, and S. Krimm, J. Mol. Struct. **159**, 183 (1987); (p) N. Makri and W. H. Willer, J. Chem. Phys. **91**, 7 (1989).
[8]S. Hayashi, J. Uemura, S. Kato, and K. Morokuma, J. Phys. Chem **88**, 1330 (1984).
[9]Y. T. Chang, Y. Yamaguchi, W. H. Miller, and H. F. Schaefer III, J. Am. Chem. Soc. **109**, 7245 (1987).
[10](a) K. Fukui, J. Phys. Chem. **74**, 4161 (1970); (b) in *The World of Quantum Chemistry*, edited by R. Daudel and B. Pullman (Dordrecht, Netherlands, 1974); (c) Acc. Chem. Res. **14**, 368 (1981).
[11]J. Bicerano, H. F. Schaefer III, and W. H. Miller, J. Chem. Phys. **78**, 259 (1983).
[12]T. Carrington and W. H. Miller, J. Chem. Phys. **84**, 4364 (1986).
[13]N. Shida, P. F. Barbara, and J. E. Almlöf, J. Chem. Phys. **91**, 4061 (1989).
[14](a) D. G. Truhlar and B. C. Garrett, Acc. Chem. Res. **13**, 440 (1980); (b) Ann. Rev. Chem. **35**, 159 (1984).
[15](a) D. G. Truhlar, A. D. Isaacson, R. T. Skodje, and B. C. Garrett, J. Chem. Phys. **86**, 2252 (1982); (b) B. C. Garrett, D. G. Truhlar, A. F. Wagner, and T. H. Dunning, Jr. **78**, 4400 (1983); (c) R. T. Skodje, D. W. Schwenke, D. G. Truhlar, and B. C. Garrett, J. Am. Chem. Soc. **88**, 628 (1984); (d) F. B. Brown, S. C. Tucker, and D. G. Truhlar, J. Chem. Phys. **83**, 4451 (1985); (e) B. C. Garrett, N. Abusalbi, D. J. Kouri, and D. G. Truhlar, *ibid.* **83**, 2242 (1985); (f) B. C. Garrett, D. G. Truhlar, J. M. Bowman, and A. F. Wagner, J. Phys. Chem. **90**, 4305 (1986); (g) G. C. Hancock, P. R. Rejto, R. Steckler, F. B. Brown, D. W. Schwenke, and D. G. Truhlar, J. Chem. Phys. **85**, 4997 (1986); (i) T. Joseph, R. Steckler, and D. G. Truhlar, *ibid.* **87**, 7036 (1987).
[16]W. H. Miller, J. Am. Chem. Soc. **101**, 6810 (1979).
[17]W. H. Miller, B. A. Ruf, and Y. T. Chang, J. Chem. Phys. **89**, 6298 (1988).
[18]E. B. Wilson, Jr., J. G. Decius, and P. C. Cross, *Molecular Vibrations* (McGraw-Hill, New York, 1955), Chap. 4.
[19]D. P. Chong and S. R. Langhoff, J. Chem. Phys. **84**, 5606 (1986); The original CPF method is described in R. Ahlrichs, P. Scharf, and C. Ehrhardt, J. Chem. Phys. **92**, 890 (1985).
[20]H. Tatewaki and S. Huzinaga, J. Comput. Chem. **3**, 205 (1980).
[21]The orbital exponents and atomic SCF orbitals used were those given in F. B. Duijneveldt, IBM J. Res. Dev. **945** (1971).
[22]J. Almlöf and P. R. Taylor, J. Chem. Phys. **86**, 4070 (1987).
[23]SIRIUS is a second order SCF-MCSCF program system developed by H. J. Aa. Jensen, H. Ågren, and P. Jørgensen.
[24]ABACUS is a property program system of SIRIUS for geometry optimizations and normal vibrational analysis. In ABACUS, analytical nuclear gradients vectors and Hessian matrices are calculated from SCF-MCSCF wave functions. The program code was developed by T. U. Helgaker, P. Jørgensen, H. J. Aa. Jensen, and P. R. Taylor.
[25]MOLECULE/SWEDEN is a vectorized SCF-MCSCF-CI-(M)CPF program system developed by P. E. M. Siegbahn, C. W. Bauschlicher, Jr., B. Roos, P. R. Taylor, A. Heiberg, J. Almlöf, S. R. Langhoff, and D. P. Chong.
[26]VIBR4 is a vibrational MCSCF program system developed by N. Shida.
[27]E. R. Davidson, in *The World of Quantum Chemistry*, edited by R. Daudel and B. Pullman (Dordrecht, Netherlands, 1974).
[28]N.Sato and S. Iwata, J. Chem. Phys. **89**, 2932 (1988).
[29](a) D. K. Hoffman, R. S. Nord, and K. Ruedenberg, Theor. Chim. Acta. **69**, 265 (1986); (b) P. Jørgensen, H. J. Aa. Jensen, and T. Helgaker, Theor. Chim. Acta. **73**, 55 (1988); (c) N. Shida, J. E. Almlöf, and P. F. Barbara, Theor. Chim. Acta. **76**, 7 (1989).
[30]For a recent review, see D. G. Truhlar and B. C. Garrett, J. Chim. Phys. **84**, 365 (1987); and references therein.